This is a repository copy of *Improved Synchronverters with Bounded Frequency and Voltage for Smart Grid Integration*.

White Rose Research Online URL for this paper:
https://eprints.whiterose.ac.uk/99434/

Version: Accepted Version

eprints@whiterose.ac.uk
https://eprints.whiterose.ac.uk/

Improved Synchronverters with Bounded Frequency and Voltage for Smart Grid Integration

Qing-Chang Zhong, *Senior Member, IEEE,* George C. Konstantopoulos, *Member, IEEE,*
Beibei Ren, *Member, IEEE,* and Miroslav Krstic, *Fellow, IEEE*

Abstract—Synchronverters are grid-friendly inverters that mimic conventional synchronous generators and play an important role in integrating different types of renewable energy sources, electric vehicles, energy storage systems, etc., to the smart grid. In this paper, an improved synchronverter is proposed to make sure that its frequency and voltage always stay within given ranges, while maintaining the function of the original synchronverter. Furthermore, the stability region characterised by the system parameters is analytically obtained, which guarantees that the improved synchronverter is always stable and converges to a unique equilibrium as long as the power exchanged at the terminal is kept within this area. Extensive OPAL-RT real-time simulation results are presented for the improved and the original self-synchronised synchronverters connected to a stiff grid and for the case when two improved synchronverters are connected to the same bus with one operating as a weak grid, to verify the theoretical development.

Index Terms—Synchronverters, virtual synchronous machines, stability, bounded frequency range, bounded voltage range, smart grid integration

Nomenclature

P_s, Q_s	real and reactive power of the synchronverter
E	RMS synchronverter voltage
V_g	RMS grid voltage
V_n	RMS rated voltage
ω	synchronverter angular frequency
ω_g	grid angular frequency
$\omega_n, \dot{\theta}_n$	rated angular frequency
δ	power angle
i_f	field-excitation current
i_{fn}	rated field-excitation current
T_e	electromagnetic torque
T_m	(virtual) mechanical torque
P_{set}, Q_{set}	real and reactive power references
D_p	frequency droop coefficient
D_q	voltage droop coefficient
M_f	maximum mutual inductance
J	(virtual) moment of inertia
τ_f	time constant of the frequency loop
τ_v	time constant of the voltage loop
$G + jB$	complex admittance between the synchronverter and the grid
$G_s + jB_s$	shunt complex admittance of the synchronverter
$G_g + jB_g$	shunt complex admittance of the grid
$\Delta\omega_{max}$	maximum angular frequency deviation
Δi_{fmax}	maximum field-excitation current deviation
p_c	maximum percentage of the voltage deviation

I. Introduction

NOWADAYS, due to the rapid increase of renewable energy systems in the electrical grid, distributed generation (DG) units play a more and more important role in power system operation. Their integration is achieved using power electronic converters and hence, the control design of power converter-fed units connected to the grid has become a major issue in control and power research communities [1], [2].

Since most of the conventional power plants are connected to the electrical grid through synchronous generators, several researchers have proposed control strategies for the power electronic inverters of distributed generation units to mimic some aspects of the conventional synchronous generators [1]–[11], mainly the external functions of synchronous generators via droop control. A different approach for inverters to provide grid support is to use electric springs [12]. Nevertheless, traditional droop controllers lack of inertia and when applied to the increasing number of renewables connected to the grid, they directly affect the stability of the power network. To this end, virtual synchronous generators (VSGs) have been proposed to introduce the droop control with an inherent virtual inertia that can be adjusted according to the power system requirements [5], [13]–[17]. In particular, a comparison between the dynamic performance of VSGs and traditional droop controllers can be found in [18], [19]. The importance of the inertia for the stability of the system can be observed in [20], where frequency oscillations are damped by alternating the moment of inertia in real time.

Although different types of VSGs have been proposed in the literature, the idea of operating inverters in a grid-friendly manner in order to mimic the complete dynamic behaviour of synchronous generators was developed as the concept of

synchronverters [1], [21], [22]. One of the important advantages of the synchronverter is that some of the system parameters, such as the inertia, the friction coefficient, the field and mutual inductance, can be suitably chosen in order to improve the dynamic performance. The synchronverter represents a promising technology in various applications, such as HVDC transmission [23], [24], MMC [16], rectifier-fed loads [25], STATCOM [26], and wind power systems [27]. Furthermore, the synchronisation unit that has been believed to be indispensable for grid-tied converters has been removed for the first time to form self-synchronised synchronverters [28], which considerably reduces the complexity of the controller and improves the performance. Therefore, most of the active players (power plants, DGs and loads) that are connected to the grid can operate in the same manner, which forms a promising architecture for the next-generation smart grid[1]. This can significantly improve the stability, scalability, reliability and security of future power systems.

Although controlling power inverters as synchronverters creates a universal way of operating all power systems, the stability of synchronverters and particularly maintaining both the voltage and the frequency within given ranges have not been established yet. This is not an easy task due to the non-linearities of the controller, e.g. the calculation of the real power and the reactive power, and the coupling between the frequency and the field-excitation current loops. Although local stability results of grid connected inverters can be provided using the small-signal analysis and linearization [18], [29]–[31], the non-linear dynamics of the system make non-linear analysis essential to achieve global stability results. Recently, a non-linear control strategy with a power-damping property was proposed to guarantee non-linear system stability [6], while requiring knowledge of the filter parameters. Several approaches for maintaining the stability of synchronous generators have been proposed in the literature, which have the same dynamics with the synchronverter, but the field-excitation current is usually considered as constant [32], [33]. As a result, according to the authors' knowledge, synchronvertes that can maintain tight bounds for the output voltage and frequency and guarantee stability based on the accurate non-linear dynamic model of the system has not been solved yet. It is worth mentioning that although saturation units can be applied to maintain given bounds for the voltage and the frequency, this often leads to instability due to the problem of integrator windup [31]. To overcome this issue, anti-windup methods could be included in the controller to change the original operation but this can no longer guarantee system stability in the original form or require additional knowledge of the system structure and parameters [34], [35].

In this paper, an improved version of the synchronverter connected to the grid with an LCL filter is proposed. The non-linear model of the system is firstly derived using the Kron-reduced network approach [36]. Then, both the frequency loop and the field-excitation current loop are implemented by using a bounded controller, inspired by the bounded

integral controller recently proposed in [37]. The improved synchronverter approximates the behaviour of the original synchronverter under normal operation (near the rated value) and guarantees given bounds for both the frequency and the voltage independently from each other, without the need of additional saturation units that will complicate the proof of stability. Hence, depending on the grid voltage and the parameters of the synchronverter, the area where a unique equilibrium exists is obtained and the convergence to the equilibrium is proven for the given voltage and frequency bounds. According to the analysis, the stability of the self-synchronised synchronverter [28], where the synchronisation unit is no longer required, is proven as well. This may shed new light on establishing the stability of next-generation smart grids, which are dominated by power-electronic converters. A preliminary version of the proposed approach was presented in [38], where the bounded control structure was only implemented in the field-excitation current loop of the original synchronverter and the stability in the sense of boundedness was shown. This paper extends the method to maintain given bounds for both the field-excitation current and the frequency, which leads to a specific bound of the synchronverter voltage that is analytically calculated, and guarantees the asymptotic stability of the closed-loop system and the uniqueness of a desired equilibrium point based on non-linear dynamic modeling. Additionally, small variations of the grid voltage and frequency are also considered such as in the case of a weak grid. It should be noted that the improved version of the synchronverter presented in this paper and the stability analysis does not obsolete the existing methods; in contrary it can be combined with some of them, e.g. the alternating inertia [20], to further enhance the dynamic performance. Extensive real-time simulation results are obtained from an OPAL-RT real-time digital simulator comparing the original and the improved self-synchronised synchronverter to verify the proposed strategy under both normal and abnormal conditions (e.g., with errors in the measurement and sudden disturbances) as well as the case of two synchronverters connected to a common bus with one operating in the droop mode as a weak grid. The second scenario investigates both the stand-alone operation of the proposed method as well as the operation with a weak grid.

In this paper, the grid is initially assumed to be stiff for the stability analysis. Later, some analysis and results are presented here when the grid voltage and frequency are varying or when two improved synchronverters are connected to the same bus with one operating as a weak grid to give some flavor of this problem.

II. OVERVIEW OF SYNCHRONVERTERS

The complete dynamic model of the synchronverter consists of a power part and a control part [1], [21]. The power part of the synchronverter consists of a three-phase inverter connected to the grid through an LCL filter. Using the Kron-reduced network approach [36], the node of the capacitor bank can be eliminated, which results in the per-phase system of the synchronverter connected to the grid as shown in Fig. 1. In this representation, the synchronverter and the grid are connected

---

[1]http://smartgrid.ieee.org/september-2013/973-how-to-achieve-completely-autonomous-power-in-the-next-generation-of-smart-grids
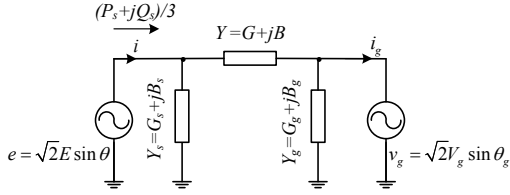
Figure 1. Per-phase diagram with the Kron-reduced network approach

via a complex admittance $Y = G + jB$ with conductance G and susceptance B, while G_s, G_g and B_s, B_g are the shunt conductance and susceptance of the synchronverter and the grid, respectively. These values can be found using the star-delta transformation of the LCL filter. Thus, the real power and reactive power at the output of the synchronverter can be found as

$$P_s = 3\left(G_s + G\right)E^2 - 3EV_g\left(G\cos\delta + B\sin\delta\right) \quad (1)$$
$$Q_s = -3\left(B_s + B\right)E^2 - 3EV_g\left(G\sin\delta - B\cos\delta\right), (2)$$

where the power angle $\delta = \theta - \theta_g$ is the phase difference between e and v_g, and it is often small [39].

The control part of the synchronverter consists of a frequency $\omega = \dot{\theta}$ loop and a field-excitation current $M_f i_f$ loop. The dynamics of the frequency ω are given by [1], [21]:

$$\dot{\omega} = \frac{1}{J}(T_m - T_e) - \frac{D_p}{J}(\omega - \omega_r), \quad (3)$$

where T_e is the electromagnetic torque (hence $P_s = T_e\omega$), T_m is the mechanical torque corresponding to the desired real output power $P_{set} = T_m\omega_n$, the reference frequency ω_r is either equal to the grid frequency $\omega_g > 0$ or to the rated frequency $\omega_n > 0$ when the frequency droop is disabled or enabled, respectively. Both J and D_p are positive constants.

The time constant of the frequency loop is given as $\tau_f = \frac{J}{D_p}$ [1] and therefore the inertia J is calculated as

$$J = D_p\tau_f, \quad (4)$$

where τ_f can be chosen similar or much smaller compared to the case of a physical synchronous generator. The dynamics of the field-excitation current i_f are given by [1], [21]:

$$\dot{i}_f = \frac{1}{KM_f}(Q_{set} - Q_s) + \frac{D_q}{KM_f}(V_n - V_g), \quad (5)$$

where K and and D_q are positive. Note that the capacitor voltage V_c, instead of V_g, can be used [21].

The time constant of the field excitation current loop is given as $\tau_v \approx \frac{K}{\omega_n D_q}$ [1] and therefore the gain K is calculated as

$$K = \omega_n D_q \tau_v, \quad (6)$$

where τ_v is often chosen much larger than τ_f. This will be further explained in Subsection III-C.

According to [1], [21] the RMS phase output voltage of the synchronverter is

$$E = \frac{\omega M_f i_f}{\sqrt{2}}. \quad (7)$$

The complete dynamic model of the synchronverter is given by (3) and (5), together with (1), (2) and (7), taking into account also that $\dot{\delta} = \omega - \omega_g$.

III. Synchronverters with Bounded Frequency and Voltage

In this section, an improved synchronverter is proposed to maintain given bounds around the rated values for the voltage and the frequency at all times (transients, disturbances, etc.) and guarantee the stability of the closed-loop system. Particularly, a bounded dynamic controller is designed for the frequency and field-excitation dynamic loops to achieve the desired bounded performance without introducing any additional saturation units or suffering from integrator windup. These continuous-time bounded dynamics allow the investigation of the area of existence of a unique equilibrium point and facilitate the stability proof for convergence to the point.

A. The proposed controller

According to utility regulations, the frequency ω of a synchronverter should be maintained within a range around the rated frequency ω_n, i.e., $\omega \in [\omega_n - \Delta\omega_{max}, \omega_n + \Delta\omega_{max}]$, where there is normally $\Delta\omega_{max} \ll \omega_n$. A common approach is to use a saturation unit at the output of the integrator (3) but this can cause integrator windup and instability [31]. In this paper, the recently proposed bounded integral controller [37] is modified to suit the needs of the frequency dynamics for the synchronverter. The frequency loop (3) is then modified and implemented as

$$\dot{\omega} = -k\left(\frac{(\omega - \omega_n)^2}{\Delta\omega_{max}^2} + \omega_q^2 - 1\right)(\omega - \omega_n) + \omega_q^2\left(\frac{1}{J}(T_m - T_e) - \frac{D_p}{J}(\omega - \omega_r)\right) \quad (8)$$

$$\dot{\omega}_q = -k\left(\frac{(\omega - \omega_n)^2}{\Delta\omega_{max}^2} + \omega_q^2 - 1\right)\omega_q - \frac{\omega_q(\omega - \omega_n)}{\Delta\omega_{max}^2}\left(\frac{1}{J}(T_m - T_e) - \frac{D_p}{J}(\omega - \omega_r)\right) \quad (9)$$

with the initial control states $\omega_0 = \omega_n$, $\omega_{q0} = 1$, and k being a positive constant gain.

In order to understand the controller (8)-(9), consider the Lyapunov function

$$W = \frac{(\omega - \omega_n)^2}{\Delta\omega_{max}^2} + \omega_q^2. \quad (10)$$

Taking the time derivative of W while considering (8)-(9), it results after some calculations in

$$\dot{W} = -2k\left(\frac{(\omega - \omega_n)^2}{\Delta\omega_{max}^2} + \omega_q^2 - 1\right)W.$$

Given the initial conditions $\omega_0 = \omega_n$ and $\omega_{q0} = 1$, there is

$$\dot{W} = 0 \Rightarrow W(t) = W(0) = 1, \forall t \geq 0.$$

Hence, ω and ω_q will start and stay thereafter on the ellipse

$$W_\omega = \left\{\omega, \omega_q \in R : \frac{(\omega - \omega_n)^2}{\Delta\omega_{max}^2} + \omega_q^2 = 1\right\}.$$

Note that the ellipse W_ω is centered at $(\omega_n, 0)$ on the $\omega - \omega_q$ plane as shown in Fig. 2(a), which means the frequency is bounded within a range around the rated value, i.e. $\omega \in [\omega_n - \Delta\omega_{max}, \omega_n + \Delta\omega_{max}]$, independently from the field-excitation current i_f and the function $\frac{1}{J}(T_m - T_e) - \frac{D_p}{J}(\omega - \omega_r)$ that needs to be regulated to 0.

Using the mathematical transformation $\omega = \omega_n + \Delta\omega_{max}\sin\phi$ and $\omega_q = \cos\phi$ and taking into account that ω and ω_q operate on W_ω, then from (8) it yields

$$\dot{\phi} = \frac{\omega_q}{\Delta\omega_{max}}\left(\frac{1}{J}(T_m - T_e) - \frac{D_p}{J}(\omega - \omega_r)\right), \quad (11)$$

which means that ω and ω_q will travel on W_ω with angular velocity $\dot{\phi}$. Hence, when $\frac{1}{J}(T_m - T_e) - \frac{D_p}{J}(\omega - \omega_r) = 0$, as required at the steady state [21], there is $\dot{\phi} = 0$ and both controller states ω and ω_q will converge at the equilibrium point (ω_g, ω_{qe}) as shown in Fig. 2(a). It should be highlighted that starting from point $(\omega_n, 1)$, both ω and ω_q are restricted only on the upper semi-ellipse of W_ω, since if at any case (e.g. during transient), the trajectory tries to reach the horizontal axis, then $\omega_q \to 0$ and from (11) there is $\dot{\phi} \to 0$ independently from the non-linear expression $\frac{1}{J}(T_m - T_e) - \frac{D_p}{J}(\omega - \omega_r)$. This means that the controller states will slow down until the system reacts, changes the sign of the angular velocity from the term $\frac{1}{J}(T_m - T_e) - \frac{D_p}{J}(\omega - \omega_r)$ and forces them to converge to the desired equilibrium. Hence, no oscillation around the whole ellipse can occur, which is an important property.
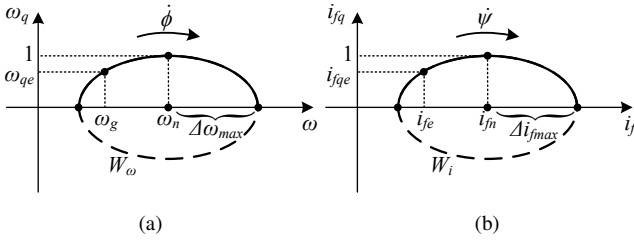

Figure 2. Phase portrait of the frequency and field-excitation current dynamics: (a) on the $\omega - \omega_q$ plane and (b) on the $i_f - i_{fq}$ plane, respectively

Since ω and ω_q operate on the upper semi-ellipse of W_ω and there are $\omega \approx \omega_n$ and $\omega_q \approx 1$ around the nominal operational point, then equation (8) becomes

$$J\dot{\omega} = \omega_q^2((T_m - T_e) - D_p(\omega - \omega_r)) \approx T_m - T_e - D_p(\omega - \omega_r). \quad (12)$$

A direct comparison of this equation with (3) implies that the proposed synchronverter approximates the dynamics of the original synchronverter around the nominal operational point, while additionally guarantees a given bound for the frequency at all times. Note also that when $\omega \to \omega_n \pm \Delta\omega_{max}$, i.e. the frequency tries to reach the upper or lower limits, then from (12) it holds that $\dot{\omega} \to 0$ which means that the integration slows down. Therefore, the proposed controller (8)-(9) inherits an anti-windup structure in a continuous-time manner that facilitates the investigation of stability, while at the same time maintains the original performance of the synchronverter around the rated values.

Utility regulations also require the RMS output voltage E of a synchronverter to be maintained within a range around the rated voltage V_n, i.e. $E \in [E_{min}, E_{max}] = [(1-p_c)V_n, (1+p_c)V_n]$, where p_c is often around 10%. In other words, according to (7), the condition

$$(1-p_c)V_n \leq \frac{\omega M_f i_f}{\sqrt{2}} \leq (1+p_c)V_n \quad (13)$$

should hold. Since the frequency ω is proven to satisfy $\omega \in [\omega_n - \Delta\omega_{max}, \omega_n + \Delta\omega_{max}]$ by (8), there is,

$$\frac{(1-p_c)V_n\sqrt{2}}{(\omega_n + \Delta\omega_{max})M_f} \leq i_f \leq \frac{(1+p_c)V_n\sqrt{2}}{(\omega_n - \Delta\omega_{max})M_f}. \quad (14)$$

This can be rewritten as

$$|i_f - i_{fn}| \leq \Delta i_{fmax}, \quad (15)$$

with

$$i_{fn} = \frac{V_n\sqrt{2}(\omega_n + p_c\Delta\omega_{max})}{M_f(\omega_n + \Delta\omega_{max})(\omega_n - \Delta\omega_{max})} \quad (16)$$

and

$$\Delta i_{fmax} = \frac{V_n\sqrt{2}(p_c\omega_n + \Delta\omega_{max})}{M_f(\omega_n + \Delta\omega_{max})(\omega_n - \Delta\omega_{max})}. \quad (17)$$

Since $\Delta\omega_{max} \ll \omega_n$ normally, there are

$$i_{fn} \approx \frac{V_n\sqrt{2}}{\omega_n M_f} \text{ and } \Delta i_{fmax} \approx \frac{p_c V_n\sqrt{2}}{\omega_n M_f}.$$

In order to achieve (15), similarly to the frequency dynamics, the field-excitation loop (5) can be modified and implemented as

$$\dot{i}_f = -k\left(\frac{(i_f - i_{fn})^2}{\Delta i_{fmax}^2} + i_{fq}^2 - 1\right)(i_f - i_{fn}) + i_{fq}^2\left(\frac{1}{KM_f}(Q_{set} - Q_s) + \frac{D_q}{KM_f}(V_n - V_g)\right) \quad (18)$$

$$\dot{i}_{fq} = -k\left(\frac{(i_f - i_{fn})^2}{\Delta i_{fmax}^2} + i_{fq}^2 - 1\right)i_{fq} - \frac{i_{fq}(i_f - i_{fn})}{\Delta i_{fmax}^2}\left(\frac{1}{KM_f}(Q_{set} - Q_s) + \frac{D_q}{KM_f}(V_n - V_g)\right) \quad (19)$$

with initial control states $i_{f0} = i_{fn}$ and $i_{fq0} = 1$.

A similar Lyapunov analysis can show that the states i_f and i_{fq} will start and stay thereafter on the ellipse

$$W_i = \left\{i_f, i_{fq} \in R : \frac{(i_f - i_{fn})^2}{\Delta i_{fmax}^2} + i_{fq}^2 = 1\right\}$$

centered at $(i_{fn}, 0)$ on the $i_f - i_{fq}$ plane, as shown in Fig. 2(b), which means the field-excitation current is bounded within the range given by (15), independently from the frequency ω and the function $\frac{1}{KM_f}(Q_{set} - Q_s) + \frac{D_q}{KM_f}(V_n - V_g)$ that needs to be regulated to 0. In the same framework, i_f and i_{fq} will travel only on the upper semi-ellipse of W_i with angular velocity

$$\dot{\psi} = \frac{i_{fq}}{\Delta i_{fmax}}\left(\frac{1}{KM_f}(Q_{set} - Q_s) + \frac{D_q}{KM_f}(V_n - V_g)\right),$$

as shown in Fig. 2(b).

The above design has actually resulted in an improved synchronverter with its frequency ω and voltage E satisfying $\omega \in [\omega_n - \Delta\omega_{max}, \omega_n + \Delta\omega_{max}]$ and $E \in [(1-p_c)V_n, (1+p_c)V_n]$, respectively. These are crucial properties for guaranteeing the system stability.

Since the given bounds are established independently from the non-linear functions of the field-excitation current loop and the frequency loop, this fact also applies to the boundedness of the self-synchronised synchronverter proposed in [28], which no longer requires a PLL. This can be achieved, as shown in Fig. 3, by replacing the dynamics of the frequency loop

and the field-excitation current loop of the self-synchronised synchronverter with the control laws (8)-(9) and (18)-(19), respectively. Since the proposed dynamics (8)-(9) and (18)-(19) introduce bounded outputs independently from the inputs (zero gain property) [37], the voltage and frequency bounds are guaranteed independently from the PI control block at the frequency loop or the first-order system used to create the virtual current i_s shown in Fig. 3.
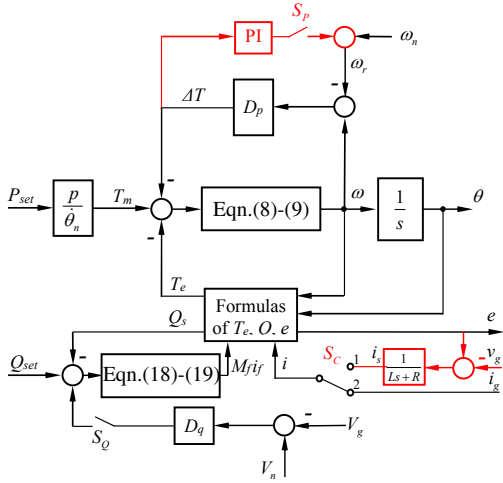

Figure 3. The control part of the proposed improved self-synchronised synchronverter

B. Existence of a unique equilibrium

It has been shown that the improved synchronverter has a bounded closed-loop solution for the frequency and the voltage (resulting from the field excitation current). Here, the existence of a unique equilibrium (with frequency ω_e and voltage E_e) and the convergence to this point will be shown analytically.

1) Theoretical analysis: Assume that the grid is stiff with constant grid voltage V_g and constant frequency ω_g to facilitate the analysis. Then, at the steady state, there should be $\omega_e = \omega_g$ because the frequency of the complete system should be the same. It has been shown that the control laws do not change the synchronverter operation at the steady state under normal operation. Then, from the equations of the improved synchronverter control part at the steady state, i.e., (18)-(19) and (8)-(9) or (5) and (3) respectively, the real power P_s and reactive power Q_s delivered by the synchronverter are

$$P_s = \frac{\omega_g}{\omega_n} P_{set} - D_p \omega_g (\omega_g - \omega_r), \quad (20)$$

$$Q_s = Q_{set} + D_q (V_n - V_g), \quad (21)$$

which are constant for given constant references P_{set}, Q_{set}.

From the controller operation, it is guaranteed that $\omega \in [\omega_n - \Delta\omega_{max}, \omega_n + \Delta\omega_{max}]$. Since $\omega_e = \omega_g$ at the steady state, the maximum frequency deviation $\Delta\omega_{max} = 2\pi\Delta f_{max}$ should be selected so that the grid frequency, which usually slightly deviates from ω_n, falls into the range $[\omega_n - \Delta\omega_{max}, \omega_n + \Delta\omega_{max}]$, although a smaller Δf_{max} can guarantee a tighter frequency bound. Usually, it is enough to choose $\Delta f_{max} = 0.5$Hz.

Moreover, the steady-state value of the voltage E_e, resulting from the field excitation current value i_{fe} and the frequency ω_e from (7), should be unique and remain inside the given range $E \in [E_{min}, E_{max}] = [(1 - p_c)V_n, (1 + p_c)V_n]$. To this end, rewrite (1) and (2) as

$$P_s - 3(G_s + G)E^2 = -3EV_g(G\cos\delta + B\sin\delta), \quad (22)$$

$$Q_s + 3(B_s + B)E^2 = -3EV_g(G\sin\delta - B\cos\delta). \quad (23)$$

Taking the sum of the squares of (22) and (23), then it yields

$$\left(P_s - 3(G_s + G)E^2\right)^2 + \left(Q_s + 3(B_s + B)E^2\right)^2 = 9E^2V_g^2\left(B^2 + G^2\right), \quad (24)$$

which results in the following second order equation of E^2 with respect to P_s and Q_s:

$$9\left((G_s + G)^2 + (B_s + B)^2\right)E^4 - \left(6P_s(G_s + G) - 6Q_s(B_s + B) + 9V_g^2\left(B^2 + G^2\right)\right)E^2 + P_s^2 + Q_s^2 = 0. \quad (25)$$

As a result,

$$E^2 = \frac{2\gamma P_s - 2\eta Q_s + 3\alpha V_g^2}{6\beta} \pm \frac{\sqrt{\Delta}}{6\beta}, \quad (26)$$

where

$$\Delta = -4(\gamma P_s + \eta Q_s)^2 + \alpha V_g^2\left(12\gamma P_s - 12\eta Q_s + 9\alpha V_g^2\right) \geq 0 \quad (27)$$

in order to obtain a real solution E_e. Here, $\alpha = B^2 + G^2$, $\gamma = G_s + G$ and $\eta = B_s + B$ with $\beta = \gamma^2 + \eta^2$. Note that for a typical LCL filter there is $\gamma > 0$ and $\eta < 0$. Since $\Delta \geq 0$, then if

$$\frac{2\gamma P_s - 2\eta Q_s + 3\alpha V_g^2}{6\beta} > 0, \quad (28)$$

the solution with the $+$ sign, denoted as E_+^2, is positive and hence, E_+ exists. The negative one $(-E_+)$ is not of interest and can be ignored. In order for E_+ to fall into the given range, there should be

$$(1 - p_c)^2 V_n^2 \leq \frac{2\gamma P_s - 2\eta Q_s + 3\alpha V_g^2}{6\beta} + \frac{\sqrt{\Delta}}{6\beta} \leq (1 + p_c)^2 V_n^2. \quad (29)$$

Since a unique solution is required in the given range, then if

$$0 < \frac{2\gamma P_s - 2\eta Q_s + 3\alpha V_g^2}{6\beta} \leq (1 - p_c)^2 V_n^2, \quad (30)$$

which includes inequality (28), then the solution with the $-$ sign, denoted as E_-^2, satisfies

$$E_-^2 \leq (1 - p_c)^2 V_n^2.$$

Hence, if E_- exists then it will be outside of the range. As a result, under conditions (27), (29) and (30), there exists a unique equilibrium E_e inside the given range $[(1 - p_c)V_n, (1 + p_c)V_n]$ with $0 \leq p_c < 1$ for the synchronverter voltage E and it is

$$E_e = E_+ = \sqrt{\frac{2\gamma P_s - 2\eta Q_s + 3\alpha V_g^2}{6\beta} + \frac{\sqrt{\Delta}}{6\beta}}.$$

Note that, when p_c is large, from (30) it may result in an area on the $P_s - Q_s$ plane that does not contain the origin $P_s = Q_s = 0$, at which $E_+ = V_g \sqrt{\frac{\alpha}{\beta}}$ and $E_- = 0$. Practically, the origin should be included to represent the operation before connecting to the grid. For $P_s = Q_s = 0$, the inequality (30) can be simplified as

$$0 \leq p_c \leq 1 - \frac{V_g}{V_n} \sqrt{\frac{\alpha}{2\beta}} < 1, \tag{31}$$

which provides a maximum practical value for p_c.

Since $P_s = Q_s = 0$ results in $E_+ = V_g \sqrt{\frac{\alpha}{\beta}}$, this also gives important information for the LCL filter design, i.e. there should be $\frac{\alpha}{\beta} \approx 1$ in order to have a smooth connection with the grid ($E_+ \approx V_g$). For the parameters in Table I, there is $\frac{\alpha}{\beta} = 1.0006$. Indeed this is the case.

Table I
SYNCHRONVERTER PARAMETERS

Parameters	Values	Parameters	Values
L_s	0.15 mH	L_g	0.15 mH
R_s	0.045 Ω	R_g	0.045 Ω
C	22 μF	nominal frequency	50 Hz
R (parallel to C)	1000 Ω	V_n	12 Vrms
rated power	100 VA	DC-link voltage	42 V

2) A numerical example: According to conditions (27), (29) and (30), for a given voltage range, the unique solution E_e of the synchronverter voltage inside the voltage range can be calculated from the values of P_s and Q_s. Then the area where there exists a unique equilibrium can be plotted on the $P_s - Q_s$ plane. In order to demonstrate this further, the system with parameters given in Table I is taken as an example. Both solutions E_+ and E_- are plotted for different values of P_s and Q_s and shown in Fig. 4. The white curve between the surfaces of E_+ and E_- defines the values of P_s and Q_s for which $E_+ = E_-$, i.e. $\Delta = 0$.
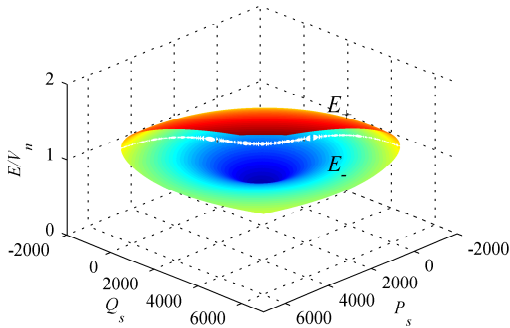

Figure 4. E_+ surface (upper) and E_- surface (lower) with respect to P_s and Q_s

The contour curves of the surface are shown in Fig. 5 on the $P_s - Q_s$ plane for $p_c = 10\%$ around the rated voltage V_n. Note that $p_c = 10\%$ satisfies (31), which gives $p_c \leq 0.2927$ when $V_g = V_n$. In the area inside the green lines, E_+ falls into the range and in the area inside the red lines E_- falls into the voltage range. Conditions (27), (29) and

(30) characterize that the area in which there exists a unique equilibrium point $E_+ = E_e$ and is inside the area between the green lines and below the gray dashed line in Fig. 5. The area where E_- exists is excluded by the gray dashed line because it would lead to excessive power that exceeds the capacity of the synchronverter.
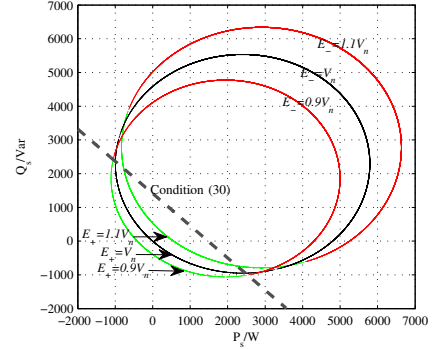

Figure 5. Illustration of the area where E_+ (inside the green lines) and E_- (inside the red lines) exist and fall inside the voltage range

The area where there exists a unique equilibrium E_e inside the voltage range is zoomed in and shown in Fig. 6(a) for two different voltage ranges with $p_c = 0.05$ and $p_c = 0.1$, i.e. 5% or 10% around the rated voltage V_n, respectively, when the grid voltage is equal to the rated voltage ($V_g = V_n$). The 5% range corresponds to the area within the blue lines, while the 10% range corresponds to the area within the green lines.

When the grid voltage is 5% lower than the rated voltage, the area where there exists a unique equilibrium E_e inside the voltage range is shown in Fig. 6(b). It can be seen that the area is shifted towards the first quadrant, which means for the same voltage range more power could be sent out but less power could be drawn. This is expected and reasonable. When the grid voltage is 5% higher than the rated voltage, the area shifts towards the third quadrant, as shown in Fig. 6(c). Hence, in practice, when determining the capacity of the synchronverter the maximum variation of the grid voltage should be taken into account as well. This provides a flavor of the weak-grid case where the grid RMS voltage can slightly vary.

C. Convergence to the equilibrium

Based on the analysis of Subsections III-A and III-B with P_s and Q_s satisfying conditions (27), (29) and (30), it has been shown that by using the improved synchronverter (8)-(9) and (18)-(19), it is guaranteed that the synchronverter connected to the grid results in a bounded voltage $E(t)$ and frequency $\omega(t)$ in a given range where a unique equilibrium (E_e, ω_e) exists. Additionally, by choosing $\tau_f \ll \tau_v$, then according to [40, Chapter 11], the frequency and field excitation current dynamics can be viewed as a two-time-scale dynamic system where the frequency dynamics are fast and the field-excitation dynamics are slow with respect to each other. The stability of these dynamics can be shown below.

1) Stability of the fast dynamics: According to (3), (1) and (7), the fast frequency dynamics around the equilibrium point
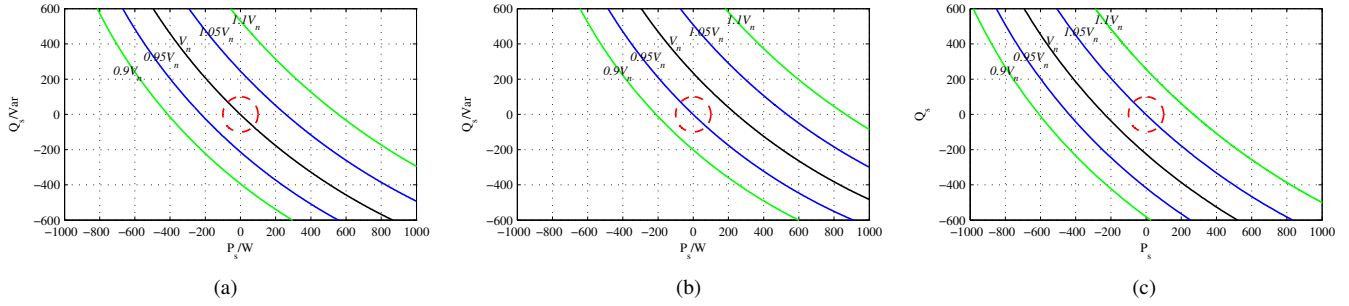
Figure 6. Illustration of the area where a unique equilibrium exists in the voltage range when the grid voltage is (a) at the rated value, (b) 5% lower than the rated value and (c) 5% higher than the rated value

(δ_e, ω_g) are given as

$$
\begin{bmatrix} \Delta\dot\delta \\ \Delta\dot\omega \end{bmatrix} = \begin{bmatrix} 0 & 1 \\ \frac{3M_f i_f V_g (B\cos\delta_e - G\sin\delta_e)}{\sqrt{2}J} & -\left(\frac{D_p}{J} + \frac{3(G_s+G)M_f^2 i_f^2}{2J}\right) \end{bmatrix} \begin{bmatrix} \Delta\delta \\ \Delta\omega \end{bmatrix},
\tag{32}
$$

because according to the two-time-scale analysis and the boundedness of i_f from (18), $i_f > 0$ and can be regarded as a constant with respect to ω. Hence, for $\delta_e \in \left(\tan^{-1}\left(\frac{B}{G}\right), \frac{\pi}{2}\right]$, the equilibrium point of the fast frequency dynamic system (32) can be easily proven to be asymptotically stable uniformly in i_f because i_f is restricted in a positive set. Note that $B < 0$ for typical LCL filters. Based on the fact that the bounded system (8) maintains the asymptotic behavior of the original system [37] with a given tight bound for the frequency ω, the equilibrium point of the fast frequency dynamics (8) is asymptotically stable since $\omega, \omega_g \in [\omega_n - \Delta\omega_{max}, \omega_n + \Delta\omega_{max}]$, i.e., the equilibrium point exists inside the given bound.

2) Stability of the slow dynamics: Once the frequency settles down quickly, according to (32), there is $\dot\delta = 0$ and $\dot\omega = 0$. As a result, $\omega = \omega_g$. For the field excitation dynamics (18)-(19), the slow dynamics of i_f in (18)-(19) result in an autonomous system $\left[\dot i_f\ \dot i_{qf}\right]^T = f\left(i_f, i_{qf}\right)$ having the same equilibrium point as the original non-linear system, because it is unique inside the bounded range. The structure of the field excitation current (18)-(19) prohibits the existence of limit cycles across the whole closed curve W_i, as explained in Subsection III-A, and the fact that i_f and i_{fq} operate on the ellipse W_i and stay exclusively above the horizontal axis, i.e. $i_{fq} \geq 0$. If i_f and i_{fq} pass the equilibrium point and try to reach the horizontal axis, as shown in Fig. 2(b), their angular velocity approaches zero, i.e. they slow down until the system acts and changes the sign of the angular velocity, forcing the states to oscillate around the equilibrium point and not continuously oscillate around the whole ellipse W_i. As a result, the field-excitation current dynamics (18)-(19) are described by a second-order autonomous system which cannot have a periodic solution, corresponding to a closed orbit on the $i_f - i_{fq}$ plane. Additionally, no chaotic solution exists according to the Poincare-Bendixon theorem [41] and the solution of the system asymptotically converges to the unique equilibrium point (i_{fe}, i_{fqe}) corresponding to the desired equilibrium of the system with (E_e, ω_e) [40].

As a result, for $\tau_f \ll \tau_v$ and for P_s and Q_s given

from (20)-(21) and satisfying conditions (27), (29) and (30), which can be achieved from the synchronverter design, the improved grid-connected synchronverter is stable with given bounds for the voltage $E \in [(1 - p_c)V_n, (1 + p_c)V_n]$ and the frequency $\omega \in [\omega_n - \Delta\omega_{max}, \omega_n + \Delta\omega_{max}]$ and asymptotically converges to a unique equilibrium point, when $\omega_g \in [\omega_n - \Delta\omega_{max}, \omega_n + \Delta\omega_{max}]$ and p_c satisfies (31).

In practice, the capacity of a synchronverter, which can be represented as a circle centered at the origin of the $P_s - Q_s$ plane, is limited and pre-defined at the design stage. If this circle, e.g. the ones shown in red in Fig. 6, falls into the area where a unique equilibrium exists, then the stability of the synchronverter is always guaranteed within the voltage range. If the real power and/or the reactive power of the synchronverter exceed the circle but still remain inside the bounded voltage area then the synchronverter is still stable but it could damage the synchronverter itself. In order to avoid damage due to overloading, the power handled by the synchronverter should be limited, e.g. to 125% for 10 minutes, 150% surge for 10 seconds. This is an excellent property that could be adopted to enhance the fault-ride through capability of grid-connected inverters, e.g. when there is a need to send (controlled) reactive power to the grid in case of a fault on the grid and to maintain the safe operation of power systems. This offers the potential for all synchronverters to work at the maximum capacity without causing instability issues.

IV. VALIDATION VIA REAL-TIME SIMULATIONS

A. One synchronverter connected to a stiff grid

In order to verify the proposed strategy, the original grid-tied self-synchronised synchronverter as reported in [28] is compared to the improved self-synchronised synchronverter shown in Fig. 3 using an OPAL-RT real-time digital simulator. The system parameters are the same as those shown in Table I and the scenario tested is the same as the one described in [28] to facilitate direct comparison. The controller parameters are chosen as $k = 1000$, $\Delta i_{fmax} = 0.15 i_{fn}$ (15% difference of the rated value) and $\Delta\omega_{max} = \pi$ rad/s, i.e., $\Delta f_{max} = 0.5$ Hz. This leads to $E_{max} \approx 1.15V_n$ and $E_{min} \approx 0.85V_n$ as the upper and lower bounds for the synchronverter voltage.

The system starts operating in the self-synchronization mode with $P_{set} = 0$ and $Q_{set} = 0$ at $t = 5$ s, with the switch S_C (Fig. 3) set at Position 1, S_P turned ON, S_Q
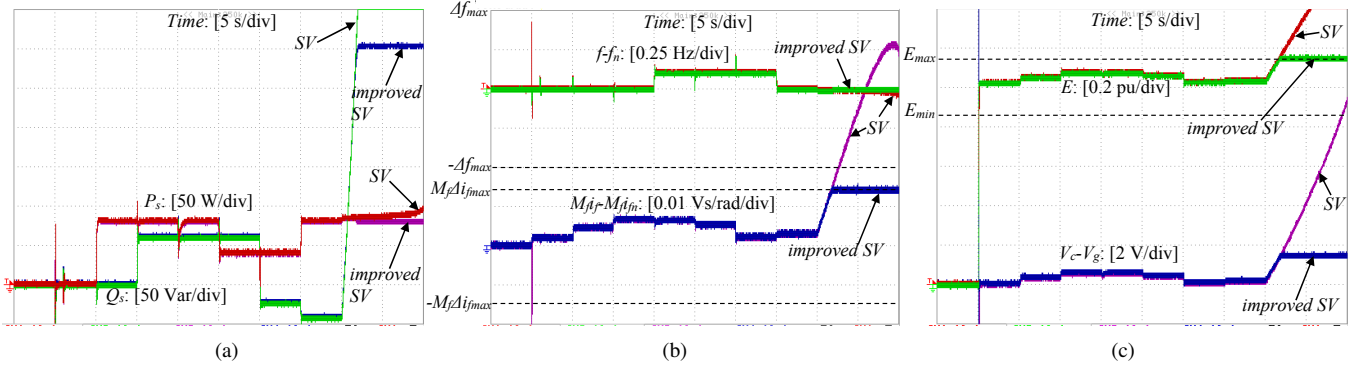
Figure 7. Real-time simulation results comparing the original (SV) with the improved self-synchronised synchronverter (improved SV): (a) real power P_s and reactive power Q_s, (b) frequency f and field-excitation current ($M_f i_f$) and (c) voltage E (normalised) and the amplitude $V_c - V_g$

turned OFF and the circuit breaker turned OFF. The initial transient observed is due to the initial conditions and the calculation of the amplitude but it does not affect the system since both synchronverters have not been connected to the grid yet. Note that the grid voltage is set to be 2% higher than the rated value in order to test the case where the grid voltage differs from the rated voltage. As it can be seen from Fig. 7(b), during the self-synchronisation mode, the synchronverter frequency is quickly synchronised with the grid frequency. At $t = 6$ s, the circuit breaker is turned ON, thus connecting the synchronverter to the grid, and S_C is changed to Position 2. Very little transient is observed. At $t = 10$ s, the real power reference is changed to $P_{set} = 80$ W and at $t = 15$ s, the reactive power reference is changed to $Q_{set} = 60$ Var. Both types of synchronverters respond to the reference values well, as shown in Fig. 7(a). At $t = 20$ s, a 0.2% step increase at the grid frequency f_g, i.e., from 50 Hz to 50.1 Hz, is assumed. Both types of synchronverters respond to the frequency change well. The transient change in the real power is small. At $t = 25$ s, Switch S_P is turned OFF to enable the frequency droop mode, which leads to a drop of the real power P_s. Switch S_Q is turned ON at $t = 30$ s to enable the voltage droop mode, which results in a drop of the reactive power Q_s. This forces the synchronverter voltage to regulate closer to the rated value (1 pu) as it is clearly shown in the normalised voltage amplitude E in Fig. 7(c). At $t = 35$ s, the grid frequency is changed back to 50 Hz. Both synchronverters behave similarly to increase the real power. Actually, during the first 40 s, both the original and the improved synchronverter have behaved almost the same, which verifies the fact that the improved synchronverter maintains the original performance during normal operation. At $t = 40$ s, an increasing error is assumed at the grid voltage sensor with the rate of $10\%/sec$, i.e. the measured voltage becomes $10\%/sec$ less than its actual value, which constitutes an abnormal operation and forces the power to increase, leading the original synchronverter to instability. As shown in Fig. 7(b), the frequency of the original synchronverter starts diverging away from the grid frequency, and the field-excitation current increases dramatically. On the other hand, the frequency and the field-excitation current of the improved synchronverter remain inside the given bounded range as expected. Particularly, the field excitation current
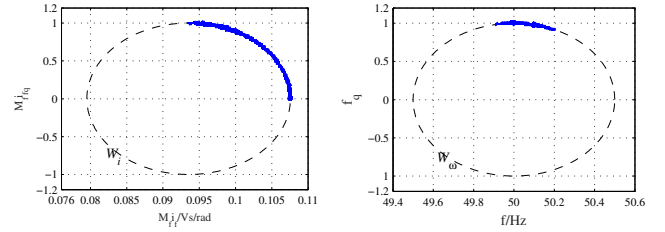

Figure 8. Phase portraits of the proposed controller states for the field-excitation loop ($M_f i_f$) and the frequency loop (f)
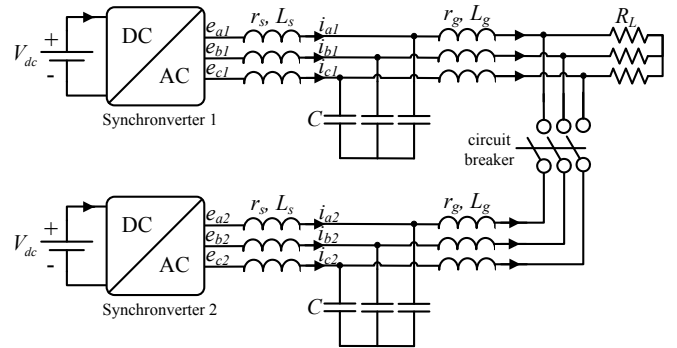

Figure 9. Two synchronverters connected to the same bus

and the voltage smoothly converge to their upper bounds as shown in Fig. 7(b) and 7(c), respectively. The frequency of the improved synchronverter is still maintained equal to the grid frequency, opposed to the original synchronverter, and the reactive power converges to the upper limit as described in Fig. 6 due to the convergence of the field-excitation current to the upper bound. Hence, both the frequency and the field-excitation current remain inside their given bounds at all times. In order to further verify the theory, the trajectories of the control states $M_f i_f$, $M_f i_{fq}$ and $f = \frac{\omega}{2\pi}$, $f_q = \omega_q$ are shown in Fig. 8 using the data from the real-time simulations. It is shown that they indeed stay on the desired ellipses as explained in Subsection III-A.
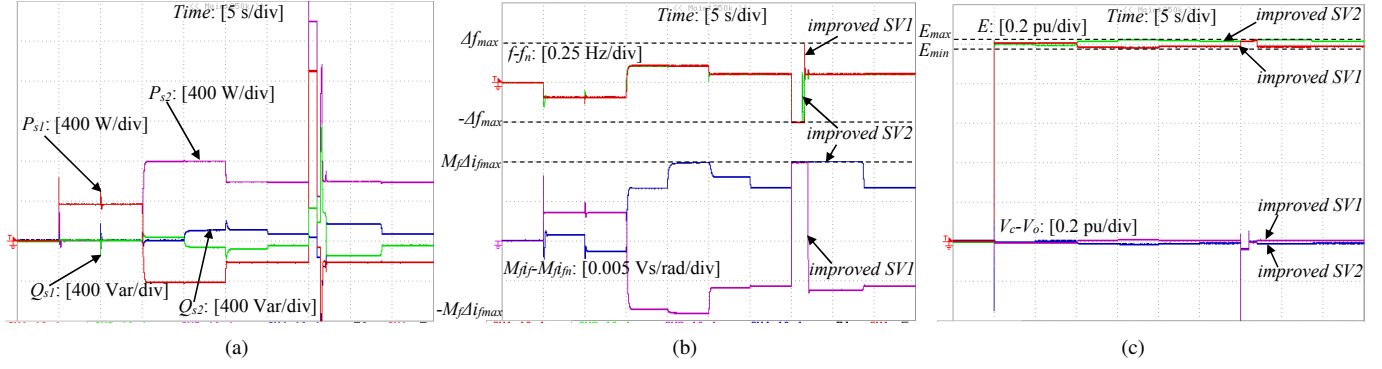
Figure 10. Real-time simulation results of two improved self-synchronverters (improved SV1 and SV2) connected at the same bus: (a) real power P_{s1}, P_{s2} and reactive power Q_{s1}, Q_{s2}, (b) frequency f and field-excitation current ($M_f i_f$) and (c) voltage E and voltage difference $V_c - V_o$ (normalised)
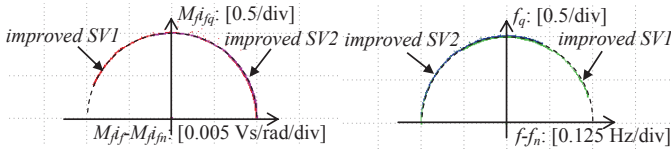

Figure 11. Controller states of the field-excitation loop ($M_f i_f$) and the frequency loop (f) for the case with two improved synchronverters connected to the same bus

Table II
SYSTEM PARAMETERS FOR THE CASE WITH TWO SYNCHRONVERTERS

Parameters	Values	Parameters	Values
L_s	2.2 mH	L_g	2.2 mH
R_s	0.5 Ω	R_g	0.5 Ω
C	22 μF	nominal frequency	50 Hz
R (parallel to C)	1000 Ω	V_n	110 Vrms
rated power	1 kVA	DC-link voltage	500 V

B. Two synchronverters connected to the same bus with one operating in the droop mode as a weak grid

To further evaluate the performance of the improved synchronverter, the case of two self-synchronised synchronverters connected to the same bus together with a local load (three-phase resistive load) is investigated using the real-time digital simulator. The diagram of the system is shown in Fig. 9. The system parameters, which are the same for both synchronverters, are shown in Table II. The maximum allowed field-excitation current deviation is chosen as $\Delta i_{fmax} = 0.02 i_{fn}$ (2% around the rated value) and the maximum frequency deviation $\Delta f_{max} = 0.25$ Hz (0.5% of the rated frequency) is used for both improved synchronverters. This leads to an approximately 2.5% range for the RMS voltage (much smaller than that in the previous simulation). The rest of the controller gains and coefficients are $k = 1000$, $D_p = 2.0264$, $D_q = 222.68$, $K = 1400$ and $J = 0.0041$, which have been obtained with the time constants $\tau_f = 0.002$ s and $\tau_v = 0.02$ s.

Initially, the first synchronverter is connected to a local load with resistance $R_L = 100 \, \Omega$ to investigate the case of stand-alone operation. With its droop functions enabled during the whole operation with $P_{set1} = 0$ W and $Q_{set1} = 0$ Var to provide frequency and voltage support, it functions as a weak grid for the second synchronverter. The system starts operating

at $t = 5$ s and both the output voltage and the frequency of improved synchronverter 1 are regulated close to the rated values due to the droop functions, as shown in Fig. 10(b). The frequency drops while the real power P_{s1} increases to feed the load and the reactive power Q_{s1} compensates the reactive power of the filter. During this period, the second synchronverter is operated in the self-synchronization mode and is synchronised very quickly with the voltage and frequency of the first synchronverter. At $t = 10$ s, the circuit breaker closes and the second synchronverter is connected to the same bus, with $P_{set2} = 0$ W, $Q_{set2} = 0$ Var in the set mode. As shown in Fig. 10(a), the real and reactive power of the second synchronverter are regulated to zero after a short and small transient. At $t = 15$ s, P_{set2} changes to $P_{set2} = 800$ W and at the time instant $t = 20$ s, $Q_{set2} = 100$ Var leading the real and reactive power of the second synchronverter to smoothly converge to the desired values. The first synchronverter acts as a weak grid and absorbs the excessive power to reach power balance, which causes the frequency to exceed the rated value. At $t = 25$ s, the frequency droop mode is enabled for the second synchronverter, leading to a drop of the real power. At $t = 30$ s, the voltage droop is enabled, forcing the reactive power to slightly drop as well. Both functions assist the frequency and the field excitation current to regulate closer to their rated values, as shown in Fig. 10(b). In order to verify the boundedness of the frequency and the voltage of the system and the stable operation under extreme scenarios, at $t = 35$ s, another three-phase load with resistance $10 \, \Omega$ is added in parallel with R_L and is disconnected at $t = 36$ s. This creates a sudden disturbance and requires excessive power from both synchronverters, as can be seen from Fig. 10(a). The field-excitation currents of both synchronverters are regulated at the maximum allowed value and the frequency at the minimum value according to the theory and hence the whole system stability is ensured, as shown in 10(b). Additionally, when the system returns to the original condition (at $t = 36$ s) then one-by-one the synchronverter frequencies and field-excitation currents return to their original values, verifying that the proposed design does not suffer from integrator windup that can destabilize the entire system. The frequencies recover much faster than the field-excitation currents, as expected. As can be seen from in 10(c), the voltage E remains within

the tight bound all the times for both synchronverters. The controller states, as shown in Fig. 11, once again, operate on the desired ellipses, verifying the theoretical development. The improved self-synchronised synchronverter can indeed maintain the voltage and frequency within given bounds at all times and guarantee the stability of the entire system under both normal and abnormal scenarios.

V. Conclusions

In this paper, an improved synchronverter with bounded frequency and voltage has been proposed. It is proven that the original behavior of the synchronverter is maintained near the rated value and additional bounds are guaranteed for the frequency and the field-excitation current (voltage). The stability and convergence to the unique equilibrium are established for a given voltage range using the non-linear model description and the complete area where the unique equilibrium exists is characterized.

Although it is assumed that the grid is stiff to derive the existence condition of an equilibrium point, the variations of the grid voltage and their effect on the desired equilibrium have been also investigated, with several real-time simulation results provided even when two synchronverters are connected to the same bus. The theoretical stability analysis for the case of practical large-scale systems with various synchronverters connected to the same network is of great significance and is being investigated.

References

[1] Q.-C. Zhong and T. Hornik, *Control of Power Inverters in Renewable Energy and Smart Grid Integration*. Wiley-IEEE Press, 2013.

[2] A. Micallef, M. Apap, C. Spiteri-Staines, J. Guerrero, and J. Vasquez, "Reactive power sharing and voltage harmonic distortion compensation of droop controlled single phase islanded microgrids," *IEEE Trans. Smart Grid*, vol. 5, no. 3, pp. 1149–1158, May 2014.

[3] J. Vasquez, J. Guerrero, A. Luna, P. Rodriguez, and R. Teodorescu, "Adaptive droop control applied to voltage-source inverters operating in grid-connected and islanded modes," *IEEE Trans. Ind. Electron.*, vol. 56, no. 10, pp. 4088–4096, Oct. 2009.

[4] Q.-C. Zhong, "Robust droop controller for accurate proportional load sharing among inverters operated in parallel," *IEEE Trans. Ind. Electron.*, vol. 60, no. 4, pp. 1281–1290, Apr. 2013.

[5] M. Ashabani and Y. A.-R. I. Mohamed, "Novel Comprehensive Control Framework for Incorporating VSCs to Smart Power Grids Using Bidirectional Synchronous-VSC," *IEEE Trans. Power Syst.*, vol. 29, no. 2, pp. 943–957, 2014.

[6] ——, "Integrating VSCs to Weak Grids by Nonlinear Power Damping Controller With Self-Synchronization Capability," *IEEE Trans. Power Syst.*, vol. 29, no. 2, pp. 805–814, 2014.

[7] M. Karimi-Ghartemani, "Universal integrated synchronization and control for single-phase dc/ac converters," *IEEE Trans. Power Electron.*, vol. 30, no. 3, pp. 1544–1557, Mar. 2015.

[8] J. Guerrero, M. Chandorkar, T. Lee, and P. Loh, "Advanced control architectures for intelligent microgrids-Part I: Decentralized and hierarchical control," *IEEE Trans. Ind. Electron.*, vol. 60, no. 4, pp. 1254–1262, Apr. 2013.

[9] A. Milczarek, M. Malinowski, and J. Guerrero, "Reactive power management in islanded microgrid-proportional power sharing in hierarchical droop control," *IEEE Trans. Smart Grid*, vol. 6, no. 4, pp. 1631–1638, July 2015.

[10] J. W. Simpson-Porco, F. Dörfler, and F. Bullo, "Synchronization and power sharing for droop-controlled inverters in islanded microgrids," *Automatica*, vol. 49, no. 9, pp. 2603–2611, 2013.

[11] G. Konstantopoulos, Q.-C. Zhong, B. Ren, and M. Krstic, "Bounded droop controller for parallel operation of inverters," *Automatica*, vol. 53, pp. 320 – 328, 2015.

[12] C. K. Lee, N. R. Chaudhuri, B. Chaudhuri, and S. Y. R. Hui, "Droop control of distributed electric springs for stabilizing future power grid," *IEEE Trans. Smart Grid*, vol. 4, no. 3, pp. 1558–1566, 2013.

[13] D. Molina, G. Kumar, G. K. Venayagamoorthy, J. Liang, and R. G. Harley, "Intelligent local area signals based damping of power system oscillations using virtual generators and approximate dynamic programming," *IEEE Trans. Smart Grid*, vol. 4, no. 1, pp. 498–508, 2013.

[14] L. M. Castro and E. Acha, "On the provision of frequency regulation in low inertia AC grids using HVDC systems," *IEEE Trans. Smart Grid*, to appear.

[15] T. Shintai, Y. Miura, and T. Ise, "Oscillation damping of a distributed generator using a virtual synchronous generator," *IEEE Trans. Power Del.*, vol. 29, no. 2, pp. 668–676, 2014.

[16] C. Li, J. Xu, and C. Zhao, "A coherency-based equivalence method for mmc inverters using virtual synchronous generator control," *IEEE Trans. Power Del.*, to appear.

[17] S. D'Arco, J. A. Suul, and O. B. Fosso, "A virtual synchronous machine implementation for distributed control of power converters in smartgrids," *Electric Power Systems Research*, vol. 122, pp. 180–197, 2015.

[18] J. Liu, Y. Miura, and T. Ise, "Comparison of dynamic characteristics between virtual synchronous generator and droop control in inverter-based distributed generators," *IEEE Trans. Power Electron.*, vol. 31, no. 5, pp. 3600–3611, 2016.

[19] A. D'Arco and J. R. Suul, "Equivalence of virtual synchronous machines and frequency-droops for converter-based microgrids," *IEEE Trans. Smart Grid*, vol. 5, no. 1, pp. 394–395, 2014.

[20] J. Alipoor, Y. Miura, and T. Ise, "Power system stabilization using virtual synchronous generator with alternating moment of inertia," *IEEE Journal of Emerging and Selected Topics in Power Electronics*, vol. 3, no. 2, pp. 451–458, 2015.

[21] Q.-C. Zhong and G. Weiss, "Synchronverters: Inverters that mimic synchronous generators," *IEEE Trans. Ind. Electron.*, vol. 58, no. 4, pp. 1259–1267, Apr. 2011.

[22] ——, "Static synchronous generators for distributed generation and renewable energy," in *Proc. of IEEE PES Power Systems Conference & Exhibition (PSCE)*, 2009.

[23] R. Aouini, B. Marinescu, K. B. Kilani, and M. Elleuch, "Synchronverter-based emulation and control of HVDC transmission," *IEEE Trans. Power Syst.*, to appear.

[24] S. Dong, Y.-N. Chi, and Y. Li, "Active voltage feedback control for hybrid multi-terminal HVDC system adopting improved synchronverters," *IEEE Trans. Power Del.*, to appear.

[25] Z. Ma, Q.-C. Zhong, and J. Yan, "Synchronverter-based control strategies for three-phase PWM rectifiers," in *Proc. of the 7th IEEE Conference on Industrial Electronics and Applications (ICIEA)*, Singapore, Jul. 2012.

[26] P.-L. Nguyen, Q.-C. Zhong, F. Blaabjerg, and J. Guerrero, "Synchronverter-based operation of STATCOM to mimic synchronous condensers," in *Proc. of the 7th IEEE Conference on Industrial Electronics and Applications (ICIEA)*, Singapore, Jul. 2012.

[27] Q.-C. Zhong, Z. Ma, W.-L. Ming, and G. C. Konstantopoulos, "Grid-friendly wind power systems based on the synchronverter technology," *Energy Conversion and Management*, vol. 89, no. 0, pp. 719–726, 2015.

[28] Q.-C. Zhong, P.-L. Nguyen, Z. Ma, and W. Sheng, "Self-synchronised synchronverters: Inverters without a dedicated synchronisation unit," *IEEE Trans. Power Electron.*, vol. 29, no. 2, pp. 617–630, Feb. 2014.

[29] N. Pogaku, M. Prodanovic, and T. Green, "Modeling, Analysis and Testing of Autonomous Operation of an Inverter-Based Microgrid," *IEEE Trans. Power Electron.*, vol. 22, no. 2, pp. 613–625, 2007.

[30] X. Guo, Z. Lu, B. Wang, X. Sun, L. Wang, and J. M. Guerrero, "Dynamic phasors-based modeling and stability analysis of droop-controlled inverters for microgrid applications," *IEEE Trans. Smart Grid*, vol. 5, no. 6, pp. 2980–2987, 2014.

[31] A. D. Paquette and D. M. Divan, "Virtual impedance current limiting for inverters in microgrids with synchronous generators," *IEEE Trans. Ind. Appl.*, vol. 51, no. 2, pp. 1630–1638, 2015.

[32] V. Natarajan and G. Weiss, "Almost global asymptotic stability of a constant field current synchronous machine connected to an infinite bus," in *2014 IEEE 53rd Annual Conference on Decision and Control (CDC2014)*, Los Angeles, CA, USA, 15-17 Dec. 2014, pp. 3272–3279.

[33] S. Fiaz, D. Zonetti, R. Ortega, J. M. A. Scherpen, and A. J. Van der Schaft, "A port-hamiltonian approach to power network modeling and analysis," *European Journal of Control*, vol. 19, no. 6, pp. 477–485, 2013.

[34] C. Bohn and D. P. Atherton, "An analysis package comparing PID anti-windup strategies," *IEEE Control Systems*, vol. 15, no. 2, pp. 34–40, 1995.

[35] L. Zaccarian and A. R. Teel, "Nonlinear scheduled anti-windup design for linear systems," *IEEE Trans. Autom. Control*, vol. 49, no. 11, pp. 2055–2061, 2004.

[36] P. S. Kundur, *Power System Stability and Control*. New York: Mc-Graw-Hills, 1994.

[37] G. C. Konstantopoulos, Q.-C. Zhong, B. Ren, and M. Krstic, "Bounded integral control of input-to-state practically stable non-linear systems to guarantee closed-loop stability," *IEEE Trans. Autom. Control*, to appear.

[38] G. Konstantopoulos, Q.-C. Zhong, B. Ren, and M. Krstic, "Boundedness of Synchronverters," in *Proc. of the European Control Conference (ECC 2015)*, Linz, Austria, July 15-17 2015, pp. 1050–1055.

[39] P. Kundur, *Power System Stability and Control*. New York, NY: McGraw-Hill, 1994.

[40] H. K. Khalil, *Nonlinear Systems*. Prentice Hall, 2001.

[41] S. Wiggins, *Introduction to Applied Nonlinear Dynamical Systems and Chaos*, 2nd ed., N. Y. Springer, Ed., 2003.

George C. Konstantopoulos (S'07-M'13) received his Diploma and Ph.D. degrees in electrical and computer engineering from the Department of Electrical and Computer Engineering, University of Patras, Rion, Greece, in 2008 and 2012, respectively.

From 2011 to 2012, he was an Electrical Engineer with the Public Power Corporation of Greece. Since 2013, he has been with the Department of Automatic Control and Systems Engineering, The University of Sheffield, U.K., where he is currently a Lecturer. His research interests include nonlinear modeling, control and stability analysis of power converters in microgrid and smart grid applications, renewable energy systems and electrical drives. Dr. Konstantopoulos is a Member of the National Technical Chamber of Greece.

Beibei Ren (S'05-M'10) received the B. Eng. degree in mechanical and electronic engineering and the M. Eng. degree in automation from Xidian University, Xi'an, China, in 2001 and 2004, respectively, and the Ph.D. degree in electrical and computer engineering from the National University of Singapore, Singapore, in 2010.

From 2010 to 2013, she was a Postdoctoral Scholar with the Department of Mechanical and Aerospace Engineering, University of California, San Diego, CA, USA. Since 2013, she has been and Assistant Professor with the Department of Mechanical Engineering, Texas Tech University, Lubbock, TX, USA. Her current research interests include adaptive control, robust control, distributed parameter systems, extremum seeking and their applications.
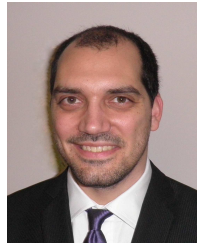
Qing-Chang Zhong (M'03-SM'04) received the Ph.D. degree in control and power engineering (awarded the Best Doctoral Thesis Prize) from Imperial College London, London, U.K., in 2004 and the Ph.D. degree in control theory and engineering from Shanghai Jiao Tong University, Shanghai, China, in 2000.

He holds the Max McGraw Endowed Chair Professor in Energy and Power Engineering at the Dept. of Electrical and Computer Engineering, Illinois Institute of Technology, Chicago, USA, and the Research Professor in Control of Power Systems at the Department of Automatic Control and Systems Engineering, The University of Sheffield, UK. He is a Distinguished Lecturer of both the IEEE Power Electronics Society and the IEEE Control Systems Society. He (co-)authored three research monographs: Control of Power Inverters in Renewable Energy and Smart Grid Integration (Wiley-IEEE Press, 2013), Robust Control of Time-Delay Systems (Springer-Verlag, 2006), Control of Integral Processes with Dead Time (Springer-Verlag, 2010), and a fourth, Power Electronics-enabled Autonomous Power Systems: Next Generation Smart Grids, is scheduled for publication by Wiley-IEEE Press. He proposed the architecture for the next-generation smart grids, which adopts the synchronization mechanism of synchronous machines to unify the interface and interaction of power system players with the grid and achieve autonomous operation of power systems. His research focuses on power electronics, advanced control theory and the integration of both, together with applications in renewable energy, smart grid integration, electric drives and electric vehicles, aircraft power systems, high-speed trains etc.

He is a Fellow of the Institution of Engineering and Technology (IET), a Senior Member of IEEE, the Vice-Chair of IFAC TC of Power and Energy Systems and was a Senior Research Fellow of the Royal Academy of Engineering/Leverhulme Trust, UK (2009-2010) and the UK Representative to the European Control Association (2013-2015). He serves as an Associate Editor for IEEE Trans. on Automatic Control, IEEE Trans. on Power Electronics, IEEE Trans. on Industrial Electronics, IEEE Trans. on Control Systems Technology, IEEE Access, IEEE Journal of Emerging and Selected Topics in Power Electronics, European Journal of Control and the Conference Editorial Board of the IEEE Control Systems Society.

Miroslav Krstic (S'92-M'95-SM'99-F'02) holds the Alspach endowed chair and is the founding director of the Cymer Center for Control Systems and Dynamics at UC San Diego. He also serves as Associate Vice Chancellor for Research at UCSD. As a graduate student, Krstic won the UC Santa Barbara best dissertation award and student best paper awards at CDC and ACC.

Krstic is Fellow of IEEE, IFAC, ASME, SIAM, and IET (UK), Associate Fellow of AIAA, and foreign member of the Academy of Engineering of Serbia. He has received the PECASE, NSF Career, and ONR Young Investigator awards, the Axelby and Schuck paper prizes, the Chestnut textbook prize, the ASME Nyquist Lecture Prize, and the first UCSD Research Award given to an engineer. Krstic has also been awarded the Springer Visiting Professorship at UC Berkeley, the Distinguished Visiting Fellowship of the Royal Academy of Engineering, the Invitation Fellowship of the Japan Society for the Promotion of Science, and the Honorary Professorships from the Northeastern University (Shenyang), Chongqing University, and Donghua University, China. He serves as Senior Editor in IEEE Transactions on Automatic Control and Automatica, as editor of two Springer book series, and has served as Vice President for Technical Activities of the IEEE Control Systems Society and as chair of the IEEE CSS Fellow Committee. Krstic has coauthored eleven books on adaptive, nonlinear, and stochastic control, extremum seeking, control of PDE systems including turbulent flows, and control of delay systems.